Dual-polarization spectral filter for radio frequency interference suppression

Laura C. Rojas[1], Dmitri N. Moisseev[1], V.Chandrasekar[1,2,3], Jason Sezler[4], Reino Keränen[5]

[1] *University of Helsinki, Erik Palmenin Aukio 1. 00014 University of Helsinki, Finland. name.lastname@helsinki.fi*
[2] *Finnish Meteorological Institute,Erik Palmnin aukio 1, 00560 Helsinki, Finland.*
[3] *Colorado State University, 1373 Campus Delivery, CO 80523,USA.chandra@engr.colostate.edu*
[4] *Vaisala Inc,7a Lyberty Way Westford, Massachusetts 01886 USA, jason.selzler@vaisala.com*
[5] *Vaisala OYj,Vanha Numijärventie 21. 01670 Vantaa, Finland. reino.keranen@vaisala.com*

(Dated: 27 May 2012)

1 Introduction

Radio local area networks (RLANs) operate in the band 5470-5725 MHz, which is also occupied by C-band weather radars. Unfortunately, some of the RLAN devices are non-compliant; they occupy the frequency even in presence of the radar signal at the same frequency band. There are numerous reports of non-compliant RLAN devices operating in Eastern Europe, South America and India. This poses challenges for meteorological services in those regions.

RLAN interference contaminate the observations in certain azimuthal angles. In severe cases sectors of tens of degrees can be affected. Ignoring observations from those angles is not the best approach because it would result in big data loss.The second best solution, after making the devices compliant, is to filter out radio frequency interference while preserving all weather echoes. Several studies have been done for filtering out ground clutter, noise and non-stationary echoes from radar observations (Dixon *et al.* 2006),(Chanthavong *et al.* 2010). In this study we demonstrate that dual-polarization spectral decomposition can be used for RF interference mitigation.

In this technique, range-velocity spectrograms are generated, and then by using image processing techniques the discrimination between different spectral lines is achieved. It was previously reported, by Moisseev and Chandrasekar (2009), that textures of differential reflectivity and differential phase and co-polar correlation spectrum can be used in the construction of a spectral filter that rejects ground clutter and noise. Using the same principle, we define an adaptive spectral filter for RLAN interference mitigation.

The methodology uses a fuzzy logic classification algorithm. The membership functions of the architecture are defined based on RLAN interference cases from Helsinki University Kumpula radar. The performance of the dual-polarization spectral filter is demonstrated on C-band radar observations from Finland, India and Brazil. The results show that the proposed filter could be a suitable solution for mitigation of RLAN interference.

2 Measurements

The data used in this study corresponds to three different C-band radar observations, which are situated in Finland (Kumpula), India (Delhi) and Brazil (Elefante). To study spectral properties of RF interference signals, dual polarization time series observations were collected from 3rd to 5th of December 2005 by Kumpula radar, located at the University of Helsinki (Finland). The presence of Radio local area networks signals was connected with the 16th OSCE Ministerial Council, which took place in Helsinki those days. To test the approach the time series of India and Brazil were superimposed, so that we have an appropriate case where both precipitation and RF interference are present. India time series were collected on 11 Jan 2012 while Brazil time series were collected on 19 Nov 2011. Both observations were in PPI mode with elevation angle of 0.5^o.

3 Methodology

The starting point of this approach is the time series data from dual-polarization radar observations, which are used to estimate the Doppler power spectrum for each polarization. Thus, for each range gate and each polarization a time series of received voltages, $V_{r_{(h/v)}}(l)$, is collected and the power spectral density can be estimated as follows (Bringi and Chandrasekar 2001)

$$\hat{S}_{(vv/hh)}[k] = \sum_{n=-M}^{M} w[n]\hat{R}_{(v/h)}[n]e^{\frac{-j2\pi nk}{N}} \tag{1}$$

where N is the number of samples, $w[n]$ is an optimized window of length $2M$, used to reduce leakage between spectral lines and minimize the amplitude error of the spectrum, and $\hat{R}[n]$ is a biased estimate of the autocorrelation function defined as (Bringi and Chandrasekar 2001).

$$\hat{R}_{(v/h)}[l] = \frac{1}{N}\sum_{n=0}^{N-l-1} V_{r_{(h/v)}}[n+l]V_{r_{(h/v)}}^{*}[n] \tag{2}$$

After implementing the power estimation, time-range averaging is applied to the estimators to reduce the estimated variance (Doviak and Zrnić 1993), and to decrease the number of samples in the processing. Thus, the averaged power estimators $\hat{S}_{A(vv/hh)}[k]$ are defined as follows:

$$\hat{S}_{A(vv/hh)}[k] = \frac{1}{M} \sum_{m=1}^{M} \hat{S}_{(vv/hh)}[k] \tag{3}$$

3.1 Spectral decompositions

From the mean sample average estimated powers for the two polarizations, $\hat{S}_{A(vv)}[k]$ and $\hat{S}_{A(hh)}[k]$, several parameters can be calculated. In this study we will concentrate in three specific parameters: differential reflectivity $\hat{Z}_d[k]$, co-polar coherency spectrum $\hat{\rho}_{hv}[k]$ and differential phase $\hat{\psi}_{dp}[k]$. They are defined as follows:

Differential reflectivity $\hat{Z}_d[k]$

This spectral decomposition is defined as the ratio in dB between the estimated power spectra for both horizontal and vertical polarizations:

$$\hat{Z}_d[k] = 10log\left[\frac{\hat{S}_{(hh)}[k]}{\hat{S}_{(vv)}[k]}\right] \tag{4}$$

Co-polar coherency spectrum $\hat{\rho}_{hv}[k]$

This polarization parameter estimate represents the correlation between the horizontal and vertical polarization channels at a given point in the space at the same time:

$$\hat{S}_{A(vv/hh)}[k] = \frac{|\hat{S}_{(hh,vv)}[k]|}{\sqrt{\hat{S}_{(hh)}[k]\hat{S}_{(vv)}[k]}} \tag{5}$$

where $\hat{S}_{(hh,vv)}[k]|$ is the cross spectrum. It is obtained by applying averaged power estimation to the cross-correlation function $\hat{R}_{hh,vv}$, which is defined as

$$\hat{R}_{(hh,vv)}[l] = \frac{1}{N} \sum_{n=0}^{N-l-1} V_{r_{(hh)}}^{*}[n+l]V_{r_{(vv)}}[n] \tag{6}$$

Differential phase $\hat{\psi}_{dp}[k]$

This spectral decomposition is the argument of the cross spectrum $\hat{S}_{(hh,vv)}[k]|$:

$$\hat{\psi}_{dp}[k] = arg\left[\hat{S}_{(hh,vv)}[k]|\right] \tag{7}$$

In this study we used these three specific parameters in creating range-velocity spectrograms for each gate. They were calculated by applying fast Fourier transform to the weighted autocorrelation functions of the time series data. These spectrograms mainly represent images. Left side of figure 1. depicts an example of these images, computed from sectors dominated by RF interference with some precipitation in the range interval of 150 to 200km.

Previous studies (Moisseev and Chandrasekar 2009) have shown that by using image processing techniques over some of these spectrograms, the discrimination between meteorological and non-weather targets is possible. This is due to the existing difference in their spectral lines. Thus, our interest is to differentiate between them, so that we are able to filter out those non meteorological signatures form the spectrum and achieve more accurate weather radar observations. For this purpose we have chosen an image texture technique, which in this case is defined as a function of the spatial variation in pixel intensities (Tuceryan and Jain 1998).

3.2 Texture calculation

Image textures are used to identify homogeneous regions, which are utilized to produce a classification map. This map is used later to define the filter. The texture is the median filter of the two-dimensional standard deviation of the image, using a 3x3 sliding window. The median filter is mainly used for reducing noise and preserving the edges of the image. Right side of figure 1 shows the co-polar coherency coefficient, ρ, and the texture, SD, of Z_d and ψ_{dp}.

As can be seen from the figure 1., there was a visual distinction between the spectral signatures of meteorological and non-weather echoes, for instance, in range around 100km. Still, the properties of these echoes have to be carefully studied to filter out those unwanted signatures in radar observations. Several studies have been carried out to do so. In our study we follow the methodology proposed by Moisseev and Chandrasekar (2009). In this approach, representative cases of precipitation, ground clutter and accurate noise estimation procedure (Chandrasekar *et al.* 1986) were considered. In each case the distributions of texture values SDZ_d, $SD\psi_{dp}$ and co-polar coherency spectrum ρ were built.
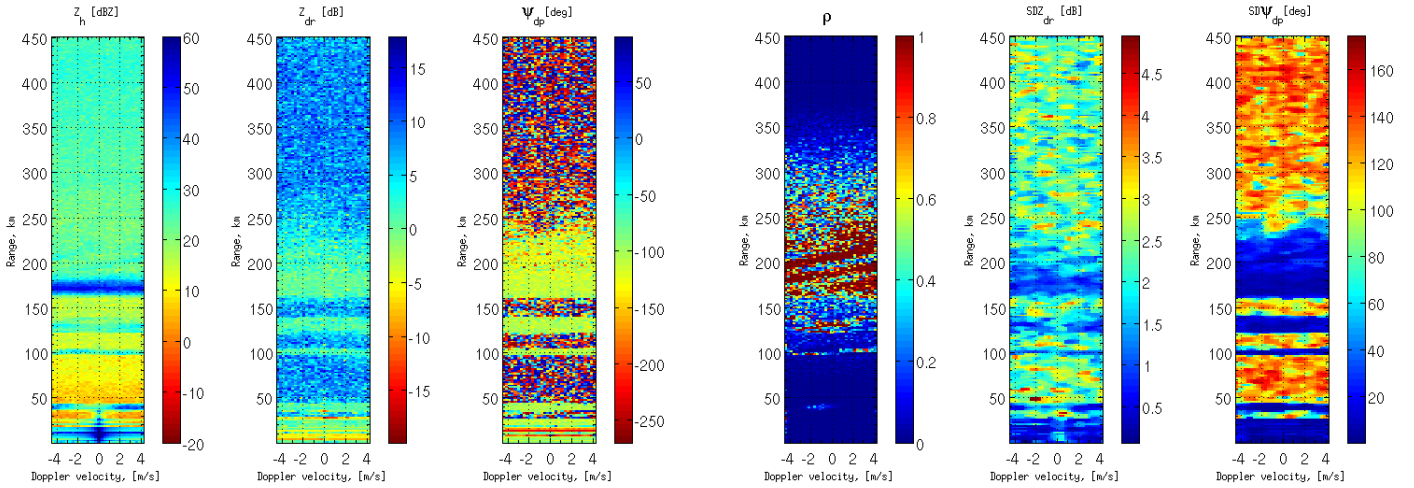
Figure 1: (Left) Power Z_h, differential reflectivity Z_{dr}, differential phase ψ_{dp} and (Right)co-polar coherency coefficient ρ and textures SDZ_{dr}, $SD\psi_{dp}$ from superimposed observations collected in India and Brazil on 11 Jan 2012 and 19 Nov 2011 respectively, at an elevation angle of 0.5^o and 35° in azimuth

Figure 2. in Moisseev and Chandrasekar (2009) presents these distributions for precipitation, ground clutter and noise. Within the principal features of the distributions can be notice that: precipitation distributions were narrow: SDZ_d values seemed to be not greater than 2dB, $SD\psi_{dp}$ values appeared not to exceed 15 degrees, and ρ values tended to be always higher than 0.9. For clutter observations the results were notably different: SDZ_d values were always greater than 2dB, $SD\psi_{dp}$ values exceeded 20 degrees, and ρ values seemed to have a very wide distribution. In the noise case the distributions appear to overlap those of precipitation and clutter. However, it can be noticed that SDZ_d values seemed to be centered around 1.5dB, a value greater than the precipitation's mean value of and lower than the one of the clutter.Also, $SD\psi_{dp}$ center value was always bigger than the center value of both precipitation and clutter, and ρ values were distributed from 0 to 0.6 with mean value of 0.2.

RF interference spectral properties

RF interference is seen by weather radars as additive white noise (Joe *et al.* 2005). Using Kumpula radar observations and following the path presented above ρ, SDZ_d and $SD\psi_{dp}$ distributions were built. Figure 2 presents the distributions for different azimuth angles where RF interference was seen.
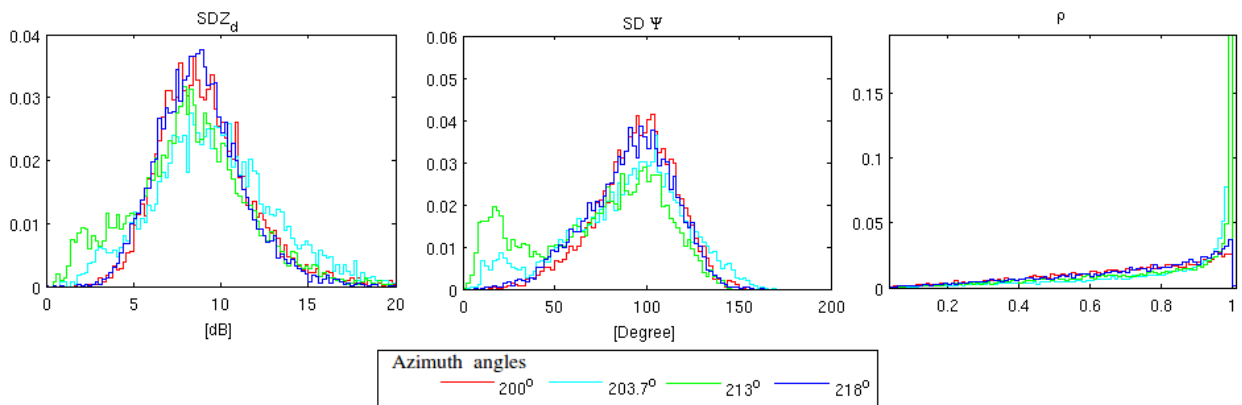

Figure 2: ρ, SDZ_d and $SD\psi_{dp}$ distributions for RF interference

As can be seen, SDZ_d values spread from 1 to 18 dB with center value being 8dB, which is greater than in the other cases. For $SD\psi_{dp}$ values a clear similarity with noise distribution was found. ρ distributions seemed to follow the shape of the one presented for precipitation, with the difference being that for RF interference the curve started to rise long before 0.9.

3.3 Classification

The difference in texture presented above suggests that we can construct classes in correspondence to the distributions of texture values and co-polar coherency coefficient. Thus, the classification process is used to evaluate whether the

received signals fulfill the properties of a certain class. For this reason, and in the same way as Moisseev and Chandrasekar (2009), a fuzzy logic classification algorithm appeared to be an appropriate classification methodology in this case.

The first step in the classification procedure was to define the membership functions, which assign each signal a grade of membership ranging between zero and one (Zadeh 1965). In this study we used the membership functions for precipitation, ground clutter and noise classes proposed by Moisseev and Chandrasekar (2009). We established the membership functions for RF interference class. In all the cases bell-shaped membership functions were used. The parameters were defined based on the distributions mentioned above, except for the precipitation (Moisseev and Chandrasekar 2009). Figure 3 shows the membership functions used.
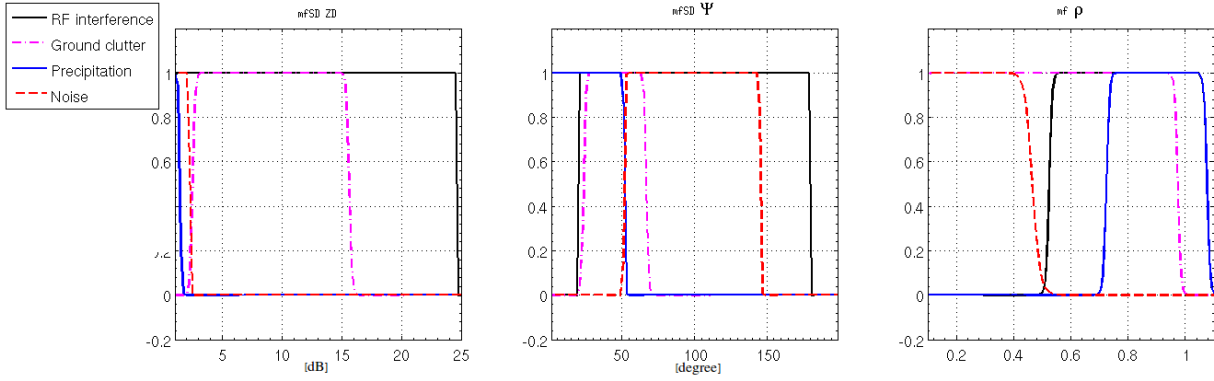

Figure 3: Membership functions for precipitation, ground clutter, noise and RF interference classes

Once the membership functions were defined, the following step was to determine the classification architecture that was going to be used. Figure 4 shows the proposed architecture. The inputs of the system were ρ, SDZ_d and
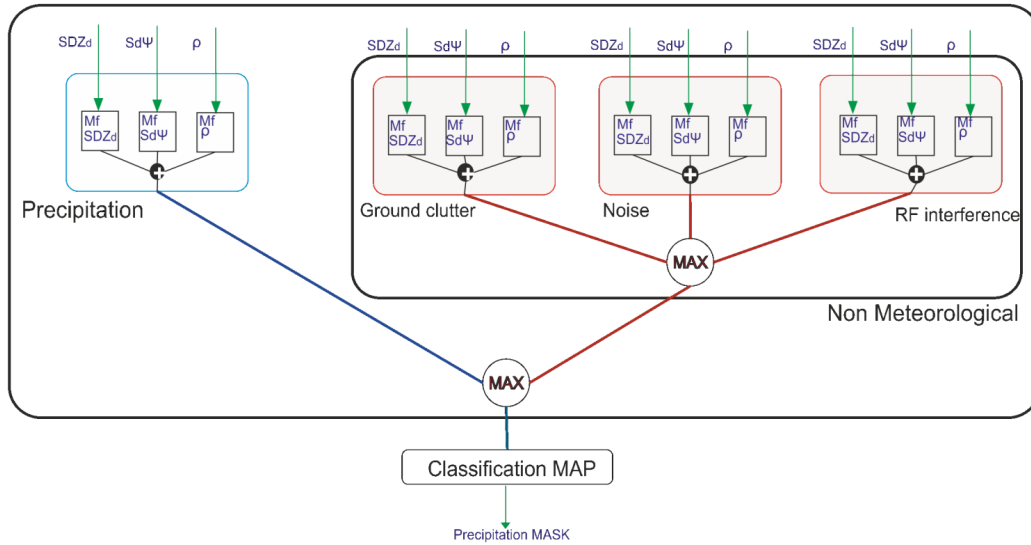

Figure 4: Classification procedure block diagram

$SD\psi_{dp}$ for each range-Doppler bin. For a given input and for each class the degree of membership was calculated, using the mentioned membership functions. The membership to certain class was determined by summing up the contributions from each fuzzy set. It is important to mention that in the same way as exposed by Moisseev and Chandrasekar (2009), for the ground clutter class a weighting factor was included to slightly force to ground clutter, when the velocities were close to zero. After finding out the degree of membership of each range-Doppler cell, what was left was to decide whether it was or not precipitation. To do so, first the membership of non-meteorological signals were compared and the maximum was selected. Then, this maximum was compared with the membership of precipitation, and the maximum value between those defined whether that cell corresponded to a meteorological or non-weather signal. Utilizing this information a classification map was built, which ended up with the creation of a precipitation mask M_k.

3.4 Moment Calculation

The last stage in the approach was to calculate the radar spectral moments. For this, first the Doppler power spectrum was noise corrected $((\hat{S}_{vv/hh}) - \sigma_N^2)$. Then a filtering was implemented using the precipitation mask,

which was equal to one if the cell was classified as precipitation or zero otherwise. By doing so, just the cells categorized as precipitation were left. And the spectral moments: reflectivity Z_h, mean velocity $\hat{v}$ and spectrum width $\hat{\sigma}_v^2$ were calculated as follows

$$Z_h = \sum_k^{N-1} \hat{S}_{vvf} \qquad \hat{v} = \frac{\sum_k^{N-1} v_k \hat{S}_{vvf}}{\sum_k^{N-1} \hat{S}_{vvf}} \qquad \hat{\sigma}_v^2 = \frac{\sum_k^{N-1} [v_k - \hat{v}] \hat{S}_{vvf}}{\sum_k^{N-1} \hat{S}_{vvf}} \tag{8}$$

where $\hat{S}_{vvf} = M_k \left[(\hat{S}_{vv}) - \sigma_N^2 \right]$, σ_N^2 is the noise power spectral density and v_k are the point velocities. The polarimetric variables can be calculated using equations 4,5 and 7 with the filtered values for $\hat{S}_{vv}$, $\hat{S}_{hh}$ and $\hat{S}_{hv}$.

To avoid possible power losses in reflectivity values, Gaussian interpolation was used over $\hat{S}_{vvf}$. The interpolation approach is similar to the one used by Siggia and Passarelli (2004).

4 Results

The dual-polarized spectral filter was tested in the radar observation mentioned before. The spectral filter appeared to work in each case, even if the radar configurations were different. Thus, according to this preliminary study the approach seems to lead to a standard model of the RF interference signals, which is independent of the location and measurement conditions. Figure 5 demonstrate the performance of the classification procedure for this data set at azimuth angle of 33°.
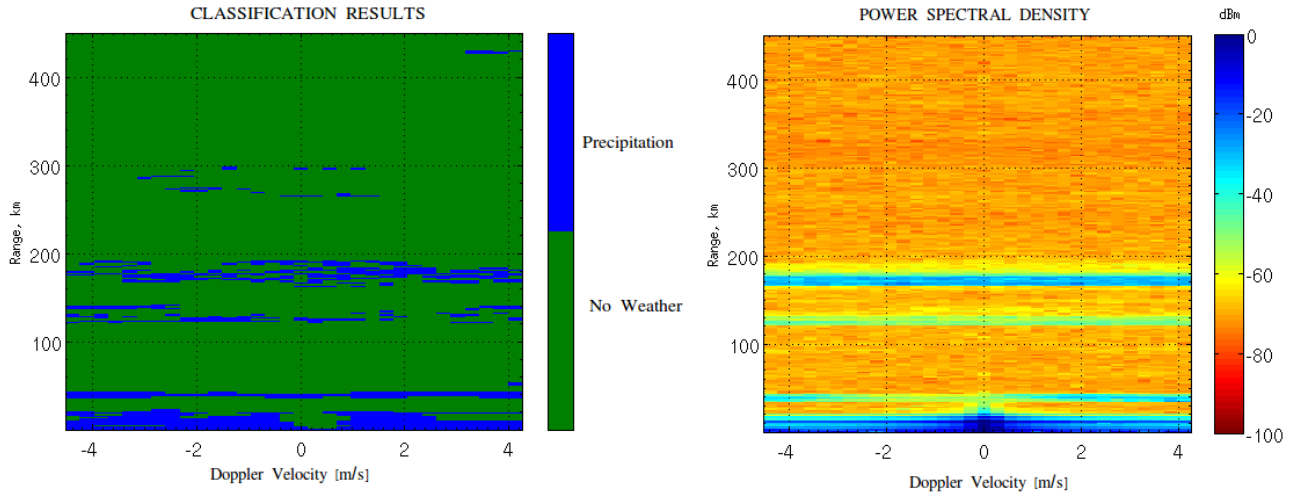

Figure 5: Classification for superimposed observations collected in India and Brazil on 11 Jan 2012 and 19 Nov 2011 respectively, at an elevation angle of 0.5^o and 33° in azimuth

As can be seen there is a good discrimination between precipitation and non-weather cells. Ground clutter, noise and RF interference appeared to be correctly classified in most of the cells. However, for some cells, due to the strong interference or the different nature of the signal, the cells are categorized as precipitation even though that was not the case. This happens for the cells in ranges larger than 250Km.

Figure 6 shows the PPI plots of the original and filtered data. This figure shows the performance of the adaptive filter. It can be seen that the RF interference signatures in most of the bins were filtered out. Although, when the RF interference was strong, for instance between 30° to 35° in azimuth, signs of the interference remained in the filtered data. In any case the observations are a lot cleaner after the filtering.

5 Conclusions

In this study we use a polarimetric spectral filter in order to improve radar observations when RF interference is present. The results show that when using this approach the radar observations and the polarimetric variables show improvement in the data quality The use of interpolation when reflectivity is calculated produces less power losses. It is important to mention that averaging and spectrum calculation using fast Fourier transform make the approach faster, which is important for the real time implementation. In this study we did classification between meteorological and non weather echoes, but classification results show that distinction between the different types of non-meteorological echoes can also be achieved.
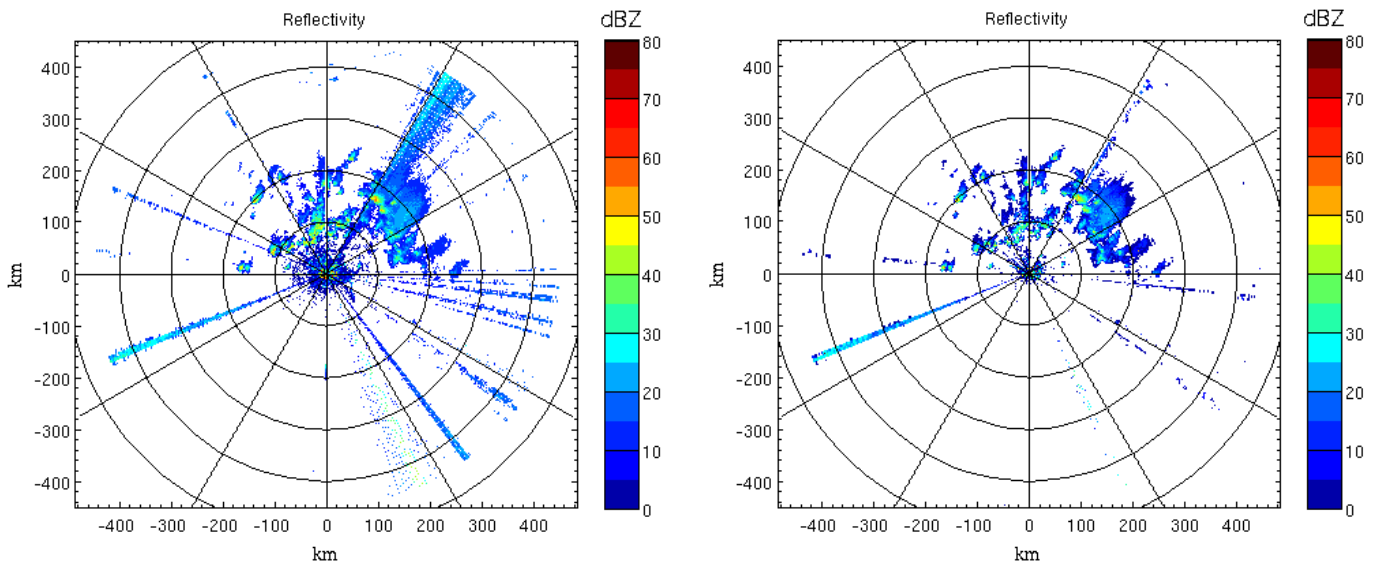
Acknowledgement

Figure 6: PPI plots before and after filter for superimposed observations collected in India and Brazil on 11 Jan 2012 and 19 Nov 2011 respectively, at an elevation angle of 0.5^o

References

Bringi, V.N., and Chandrasekar, V. 2001. *Polarimetric Doppler weather radar: principles and applications.* Cambridge University Press.

Chandrasekar, V., Bringi, V. N, and Brockwell, P. 1986. *Statistical properties of dual polarized radar signals.* 23rd conference on Radar Meteorology.

Chanthavong, V., Homes, J., Keränen, R., Doug, P., Sezler, J., Siggia, A., and Stordell, T. 2010. Mitigation of sea clutter and other non-stationary echoes based on general purpose polarimetric echo identification. *ERAD 2010 6th European conference on Radar in Meteorology and Hydrology.*

Dixon, M., Kessinger, C., and Hubbert, J.C. 2006. Echo classification within the spectral domain to discriminate ground clutter from meteorological targets. 22nd *conference on Interactive Information processing Systems for Meteorology, Oceanography and Hidrology.*

Doviak, R.J, and Zrnić, D.S. 1993. *Doppler Radar and Weather Observations.* Second edition edn. Dobler publications,INC.

Joe, P., Scott, J., Sydor, J., Brandão, A., and Yongacoglu, A. 2005. *Radio Local Area Network (RLAN) and C-Band Weather Radar Interference Studies.* 32nd AMS Radar Conference on Radar Meteorology.

Moisseev, D., and Chandrasekar, V. 2009. Polarimetric Spectral Filter for Adaptative Clutter and Noise Suppression. *Journal of atmospheric and oceanic technology*, **26**, 215–228.

Siggia, D.A, and Passarelli, R.E.Jr. 2004. *Gaussian model adaptative processing(GMAP) for improved ground clutter cancellation and moment calculation.* procedings ERAD.

Tuceryan, M., and Jain, A.K. 1998. Texture Analysis. *The Handbook of Pattern Recognition and Computer Vision.*

Zadeh, L.A. 1965. Fuzzy sets. *Information and control*, **8**, 338–353.